Research on Chemical Intermediates
https://doi.org/10.1007/s11164-019-03905-1

Catalytic activity of rare earth and alkali metal promoted (Ce, La, Mg, K) Ni/Al_2O_3 nanocatalysts in reverse water gas shift reaction

Atieh Ranjbar[1] · Abdullah Irankhah[2] · Seyed Foad Aghamiri[1]

Received: 10 January 2019 / Accepted: 14 June 2019

Abstract

Nanocrystalline Ni/Al_2O_3 catalysts and promoted Ni-M/Al_2O_3 (M = Ce, La, Mg, K) catalysts were employed a in reverse water gas shift reaction. Among the prepared nickel catalysts 5% Ni/Al_2O_3 catalyst showed high CO_2 conversion and CO selectivity. To improve the CO_2 conversion and CO selectivity of 5% Ni/Al_2O_3, 1 or 2 wt% Ce, La, Mg or K were used. One percent La and 2% K showed highest CO_2 conversion and CO selectivity. The high activity and CO selectivity of promoted catalysts can be accredited to the increase of Ni dispersion (or smaller Ni particles), concentration of surface active sites and CO_2 adsorption by basic nature of promoters. The prepared samples were characterized by X-ray diffraction, inductively coupled plasma emission spectroscopy, N_2 adsorption–desorption (BET), temperature programmed reduction (TPR), scanning electron microscopy and transmission electron microscopy (TEM) techniques. The BET surface area of prepared γ-alumina support was 126.81 $m^2\ g^{-1}$, impregnation of the support with Ni and promotion of 5 wt% Ni with K and La reduced the specific surface area. The support and catalysts possessed mesoporous structure. The TPR-H_2 analysis revealed higher Ni dispersion and reducibility for promoted nickel catalysts; 5Ni–2K showed highest reducibility. TEM images of 5Ni and 5Ni–2K showed increase of Ni dispersion and decrease of Ni particle size for the promoted catalyst. After 50 h on stream at 600 °C, 5Ni–1La and 5Ni–2K performed great catalytic stability.

✉ Abdullah Irankhah
irankhah@kashanu.ac.ir

[1] Department of Chemical Engineering, Faculty of Engineering, University of Isfahan, Isfahan, Iran

[2] Hydrogen and Fuel Cell Research Laboratory, Department of Chemical Engineering, Faculty of Engineering, University of Kashan, Kashan, Iran

Published online: 20 June 2019

Graphic abstract

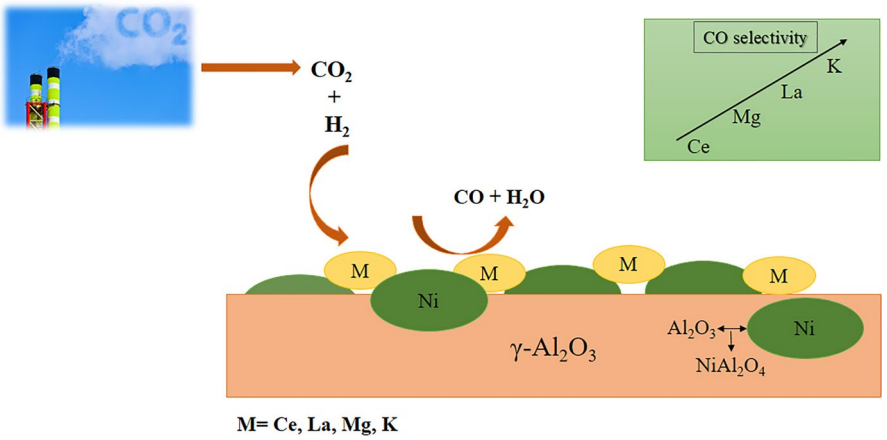

Keywords CO_2 mitigation · RWGS · Nickel catalyst · Promoter · γ-Al_2O_3

Introduction

The negative effect of CO_2 on climate change and global warming is well known. Utilization of CO_2 in catalytic reactions such as CO_2 hydrogenation can decrease its concentration in the atmosphere. Reverse water gas shift (RWGS) reaction at atmospheric pressure recycles CO_2 into CO ($CO_2 + H_2 \leftrightarrow CO + H_2O$), which is the feedstock for production of methanol (via carbon dioxide hydrogenation to form methanol via a reverse-water-gas-shift reaction, or CAMERE, process) and other valuable hydrocarbons. The catalytic reactions that directly convert CO_2 into valuable products suffer from low CO_2 conversion.

Several types of catalysts have been reported for RWGS reaction. Noble metals Pt, Rh, Au, Pd and their bimetallic combinations such as Pt–K, Au–Mo, Rh–Fe were used for the reaction [1–6]. These catalysts are active and CO-selective, but they are expensive and can't be used for large-scale CO production [7]. Cost-effective non-noble metals such as Fe, Mn, Cu, Ni, Co have also been evaluated. Fe- and Mn-based catalysts supported on Al_2O_3 and CeO_2 showed high CO selectivity, but low CO_2 conversions [8, 9]. Cu based catalysts supported on Al_2O_3, CeO_2 and SiO_2 showed better CO_2 conversions, but suffered from low thermal stability at temperatures higher than 500 °C [10]. RWGS reaction is an endothermic reaction and higher temperatures are preferred. Addition of promoters such as Fe, K, Ni to Cu-based catalysts prevented Cu particles from agglomeration at higher temperatures and induced better dispersion of Cu particles [11–13]. Ni based catalysts supported on Al_2O_3, CeO_2, SiO_2, B-Mo_2C, SBA-15 and Ce–Zr–O exhibited high CO_2 conversion,

but low CO selectivity especially at lower temperatures [14–20]. Low CO selectivity is a consequence of CO and CO_2 methanation reactions occurring along with the RWGS reaction.

$$CO_2 + 4H_2 \leftrightarrow CH_4 + 2H_2O \quad \Delta H = -252.9 \text{ kJ mol}^{-1} \tag{1}$$

$$CO + 3H_2 \leftrightarrow CH_4 + H_2O \quad \Delta H = -165.0 \text{ kJ mol}^{-1} \tag{2}$$

Addition of a basic promoter can hinder the parallel methanation reactions occurring along with the RWGS process [21]. Addition of K promoter to Ni/CeO_2 catalysts decreased CH_4 selectivity in medium-temperature shift reaction [22, 23]. A basic promoter partially blocks acidic sites available and aids the adsorption of acidic CO_2 on the created active sites [24]; consequently the formation of CH_4 during reaction is prevented. Ce, La, Ca, Mg and K or their oxides have been widely added as promoters to Ni-based catalysts for reactions such as dry reforming of methane or biogas dry reforming [25–29]. Furthermore, addition of a rare earth promoter increased the Ni dispersity and stabilized catalytic activity of Ni/Al_2O_3 catalysts at high temperatures in dry reforming of methane reaction [30, 31]. Higher Ni dispersion and smaller Ni particles increase the CO selectivity in RWGS reaction [15].

Until now addition of Ce, La, Mg and K as promoters to Ni/Al_2O_3 catalysts and their effect on the CO selectivity in RWGS reaction has not been evaluated. Different basic promoters (rare earth metal and alkali) are chosen to figure out which is more efficient for RWGS process. Before promoting the catalysts, we have also experimented Ni/Al_2O_3 catalysts with different nickel loadings to find out the proper nickel loading. The catalysts were prepared by impregnation and co-impregnation technique. The γ-alumina support used in this work was prepared by precipitation method.

Experimental

Support preparation

For preparation of Al_2O_3 appropriate amount of aluminum nitrate ($Al(NO_3)_3{\cdot}9H_2O$) is dissolved in distilled water. Ammonia was added drop wise to the solution at 30 °C by careful adjustment of pH to 7.5. After precipitation, the mixture was refluxed at 60 °C for another 12 h under stirring. The precipitate was filtered and washed with distilled water. The product was dried at 80 °C for 24 h and calcined at 700 °C for 4 h.

Preparation of Ni/Al_2O_3

Nickel catalysts were prepared by impregnation. Primarily, the prepared support was dispersed in distilled water then $Ni(NO_3)_2{\cdot}6H_2O$ was added to the solution to obtain 2, 5, 7 and 10 wt% Ni. The slurry was stirred for 4 h at room temperature. The

mixtures were dried at 100 °C for 24 h and calcined at a rate of 3 °C min^{-1} at 600 °C and kept for 4 h at the final temperature.

Preparation of Ni-M/Al_2O_3

Promoted nickel catalysts were prepared by co-impregnation. After dispersing the support in distilled water, Ni $(NO_3)_2{\cdot}6H_2O$ and the rare earth metal or alkali promoter ($Ce(NO_3)_3{\cdot}6H_2O$, $LaNO_3$, $Mg(NO_3)_2{\cdot}6H_2O$, KNO_3) were simultaneously added to the solution to obtain 5 wt% Ni and 1 or 2 wt% M where M = Ce, La, Mg or K. The slurry was stirred for 4 h at room temperature. The prepared samples were dried and calcined at the same condition as Ni/Al_2O_3 catalysts.

Characterization

The XRD patterns were recorded on an X-ray diffractometer (PANalytical X'Pert-Pro) using a Cu-Kα monochromatized radiation source and a Ni filter in the range $2\theta = 10°$ to 80°. Analyses were compared with the Inorganic Crystal Structure Database (ICSD) using powder diffraction file no. 75-1862 for Al_2O_3, no. 47-1049 for NiO, 10-0339 for $NiAl_2O_4$ and 87-0712 for Ni. The surface areas (BET) were determined by nitrogen adsorption at − 196 °C using an automated gas adsorption analyzer (Tristar 3000, Micromeritics). The total metal loading (wt%) of the calcined catalysts were determined by inductively coupled plasma atomic emission spectroscopy (ICP-OES) using Varian Vista-Pro CCD Simultaneous. Temperature programmed reduction (TPR–H_2) profiles were obtained by using Micromeritics AutoChem 2920 TPR apparatus, in temperature range from 30 to 1000 °C at a rate of 10 °C min^{-1} under flow rate of 20 ml min^{-1} of 5 vol% H_2/Ar. The catalyst samples were degassed under inert atmosphere of Ar at 200 °C prior to the TPR analysis. Scanning electron microscopy (SEM) was performed with VEGA TESCAN, operated at 30 kV for the surface morphology. SEM analysis was followed by energy dispersive spectrometry (EDS) analysis for the elemental composition. Morphological and structural characteristics of the reduced and used catalysts were also examined using a transmission electron microscope (TEM Philips CM120) operated at 120 keV.

Catalyst testing

Catalytic activity experiments were carried out in a fixed-bed continuous-flow reactor at atmospheric pressure; see Fig. 1. The reactor is made of an 8-mm-i.d. quartz tube. The reactor was charged with 200 mg catalyst for each test. Prior to the reaction, the catalyst was reduced in situ in flow of H_2 (30 ml min^{-1}) at 600 °C for 4 h and cooled down afterwards to 400 °C in a flow of an inert gas (Ar). The reactant gases consisting of H_2:CO_2 = 1:1 and (50 ml min^{-1}) were introduced into the reactor. Inlet flow of reactant gases were monitored by mass flow controllers. The activity measurement tests were carried out at temperatures ranging from 400 to 700 °C in steps of 100 °C. The experiments were repeated three times at each temperature. The

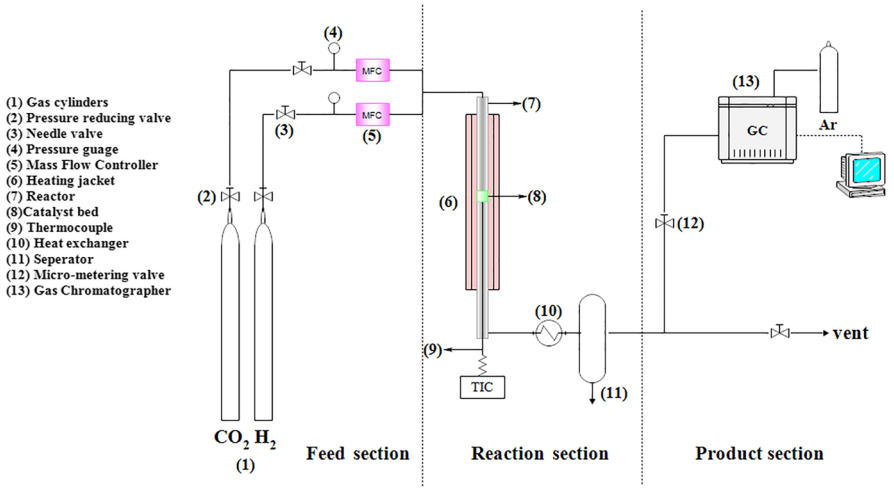

Fig. 1 Process flow diagram of experimental apparatus for reverse water gas shift reaction over Ni/Al_2O_3 catalysts and $Ni\text{-}M/Al_2O_3$ catalysts

accuracy of the tests were controlled by carbon balance ($C_{in} - C_{out} < \varepsilon$). The product stream was analyzed by a gas chromatograph equipped with thermal conductivity detector (TCD) and a Carbosieve column. The long-term stability was checked out for 50 h at 600 °C.

The CO_2 conversion, CO and CH_4 selectivity were evaluated as follows:

$$CO_2 \text{ conversion } (\%) = \left(\left[CO_2\right]_{in} - \left[CO_2\right]_{out}\right) / \left[CO_2\right]_{in} \times 100 \tag{3}$$

$$\text{Selectivity of CO } (\%) = [CO]_{out} / \left(\left[CO_2\right]_{in} - \left[CO_2\right]_{out}\right) \times 100 \tag{4}$$

$$\text{Selectivity of } CH_4 \ (\%) = \left[CH_4\right]_{out} / \left(\left[CO_2\right]_{in} - \left[CO_2\right]_{out}\right) \times 100 \tag{5}$$

Results and discussion

Catalytic characterization

Figure 2a presents the XRD patterns of prepared support and different nickel loadings on Al_2O_3. For the alumina support, formation of pure crystalline phase is evident from the peaks indexed as Al_2O_3. For nickel catalysts, no obvious peaks related to NiO are observed. NiO reflections at 37.3° and 43.3° overlap with the reflections of alumina at 37.7° and 43.3°, respectively. Addition of nickel to Al_2O_3 has reduced its crystallinity. Characteristic lines related to nickel aluminate phase ($NiAl_2O_4$) at 37.96° and 43.53° are also overlapped with alumina and NiO reflections. Figure 2b

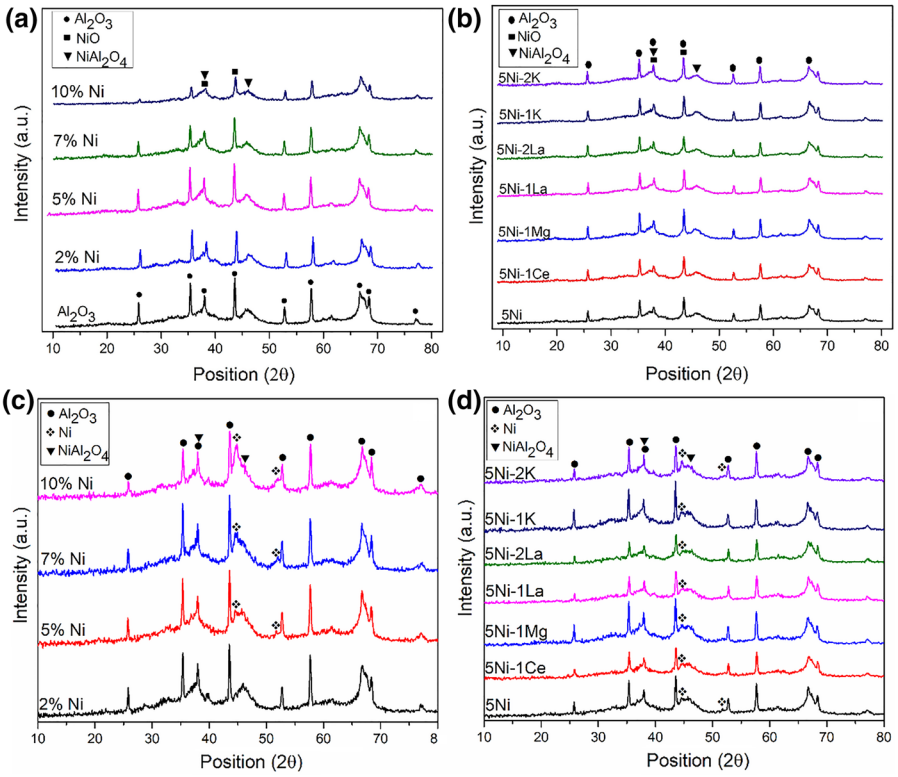

Fig. 2 XRD patterns of prepared support and catalysts; **a** Al_2O_3 and Ni/Al_2O_3 catalysts, **b** $5Ni\text{-}M/Al_2O_3$ (M = Ce, Mg, La, K) catalysts, **c** reduced Ni/Al_2O_3 catalysts and **d** reduced $5Ni\text{-}M/Al_2O_3$ (M = Ce, Mg, La, K) catalysts

shows the XRD patterns of promoted nickel catalysts. Because of the low promoter content no reflections related to promoters were detected. As it can be seen from diffractions of reduced nickel catalysts (Fig. 2c), for 5% Ni and higher loadings, peaks related to Ni at 44.49° and 51.85° are observed. The diffractograms of promoted $5Ni\text{-}M/Al_2O_3$ catalysts are shown in Fig. 2d. For these catalysts, as well as the non-reduced samples, no peaks related to promoters could be detected.

The structural properties of prepared samples are shown in Table 1. The average crystallite size of prepared support is calculated from the half-width of diffraction peaks (β) using Scherrer's formula. The prepared support showed nanocrystalline structure with average crystallite size of 31.26 nm. Ni crystallite sizes are calculated on (111) and (200) planes, also by using Scherrer's formula. Increase of Ni crystallite size is observed with increase of nickel loading. The prepared support showed higher specific surface area in comparison with the nickel catalysts and nickel promoted catalysts. The average pore diameter increased with addition of nickel and promoters to the support. Incorporation of Ni and promoters with the support declined the structure of Al_2O_3.

Table 1 Structural properties of prepared samples

Sample	D_{XRD} avg. crystallite size[a] (nm)	Ni crystallite size (nm)[a]	BET ($m^2\ g^{-1}$)	Total pore volume ($cm^3\ g^{-1}$)	Average pore diameter (nm)
Al_2O_3 support	31.3	–	126.8	0.2182	6.9
2Ni	–	–	–	–	–
5Ni	–	–	111.1	0.2215	7.9
7Ni	–	12.3	–	–	–
10Ni	–	13.8	–	–	–
5Ni–2K	–	12.4	103.1	0.2131	8.3
5Ni–1La	–	–	105.2	0.2149	8.1

[a]Calculated from the XRD patterns

Table 2 The ICP analysis of 5Ni–1La and 5Ni–2K

Sample	Ni (wt%)	La (wt%)	K (wt%)
5Ni–2K	4.22	0	1.96
5Ni–1La	4.05	0.83	0

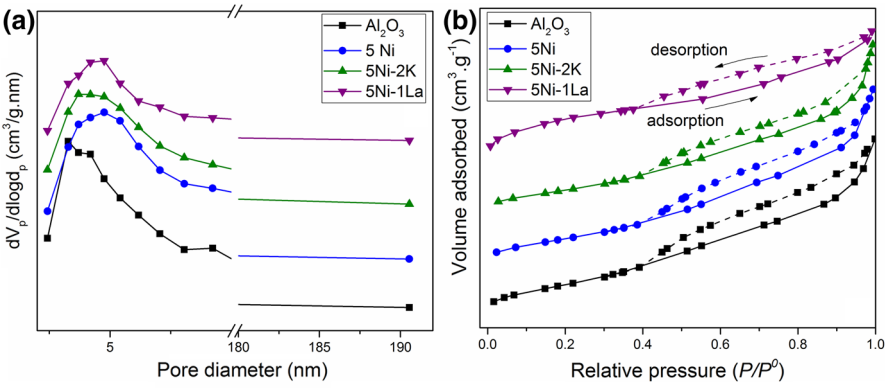

Fig. 3 **a** Pore size distributions and **b** N_2 adsorption/desorption isotherms of Al_2O_3, 5Ni/Al_2O_3, 5Ni–2K/Al_2O_3 and 5Ni–1La

The ICP results of 5Ni–1La and 5Ni–2K showed that the metal levels close to desired levels were achieved for these catalysts (see Table 2).

Figure 3a reveals the pore size distribution for Al_2O_3 support, 5Ni, 5Ni–2K and 5Ni–1La. Pore sizes calculated by the BJH method are mainly about 2–10 nm, indicating mesoporous structure for all the prepared samples. The nitrogen adsorption/desorption isotherms are shown in Fig. 3b. According to the IUPAC classification the N_2 isotherm is a type IV isotherm with a large type H3 hysteresis loop. This type of isotherm is usually given by mesoporous structures where monolayer-multilayer adsorption is followed by pore condensation (gas condenses in pores at pressure P less than P^0) [32].

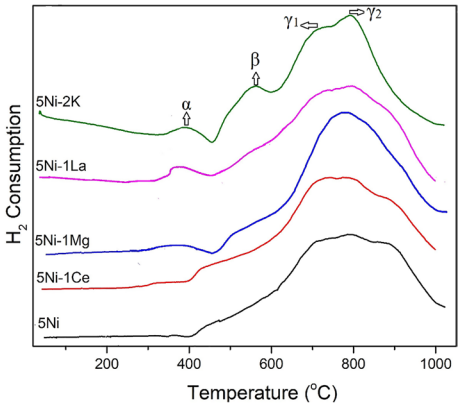

Fig. 4 TPR profiles of 5Ni/Al_2O_3, 5Ni–1Ce/Al_2O_3, 5Ni–1Mg/Al_2O_3, 5Ni–1La/Al_2O_3 and 5Ni–2K/Al_2O_3 (10% vol H_2/Ar, heating rate 10 °C min^{-1})

Table 3 Total hydrogen consumption values of 5Ni/Al_2O_3 and 5Ni-M/Al_2O_3 (M = Mg, Ce, La, K) catalysts

Catalyst	Total H_2 consumption (μmol g^{-1})
5Ni	871.2
5Ni–1Mg	969.5
5Ni–1Ce	937.7
5Ni–1La	977.7
5Ni–2K	1061.2

Figure 4 shows the TPR profiles of 5% nickel and 5% nickel promoted catalysts. The reduction is observed over a wide range of temperature from 300 to 950 °C. The peak β is related to NiO species, which have strong interaction with the support. γ_1 peak, which appears around 700 °C and is attributed to the presence of Ni^{2+} species in the octahedral coordination. γ_2 peak appearing around 800 °C and higher is assigned to Ni^{2+} species in the tetrahedral environment that corresponds to the spinel structure of $NiAl_2O_4$ [33, 34]. The peaks β, γ_1 and γ_2 are only distinguished in 5Ni–2K, and for the rest of prepared catalysts these peaks are merged together. In addition to the peaks for 5Ni–2K, 5Ni–1La and 5Ni–1Mg a small peak labeled as α at left shoulder of these profiles around 380 °C is detected, which is associated with well dispersed NiO with weak interaction to the support. Addition of promoters has increased the reduction peaks and shifted the maximum temperature of these peaks to slightly lower temperatures. The increasing reducibility of promoted Ni catalysts is confirmed by increase of H_2 consumption. Table 3 gives the total H_2 consumption of 5Ni and 5Ni-promoted catalysts. Among the prepared catalysts 5Ni–2K showed the highest H_2 consumption. The appearance of NiO species with lower interaction with the Al_2O_3 support and shifting of maximum temperature of the peaks to lower temperatures, after impregnation with alkali promoters has been reported by many researchers [25, 35–37]. Mazumder et al. showed that after impregnation of Ni/Al_2O_3 with La_2O_3, a small peak around 390 °C appeared. They illustrated that highly

dispersed NiO on the support surface was responsible for this low temperature peak [29]. The same results have also been reported for CeO_2 as promoter [38], but here we haven't seen much change in reduction of the Ce promoted catalyst, except a small temperature shift.

Figure 5 shows SEM images of Al_2O_3 support, 5% Ni/Al_2O_3 and promoted Ni catalysts. As can be seen, they don't have any particular shape. The promoted catalysts showed similar particle size distribution (an average between 60 and 90 nm) except 5Ni–1Mg, which showed larger particles among the promoted catalysts. Since we had low promoter loadings that could not be detected by XRD analysis, we used energy dispersive analysis (EDS), as shown in Table 4. All available elements in the prepared catalysts were detected by EDS analysis. The reported amounts were close to desired loadings in catalysts.

Figure 6 shows TEM images of reduced $5Ni/Al_2O_3$ and $5Ni–2K/Al_2O_3$ catalysts. Ni particles in both samples exhibit nearly spherical shaped particles and fall in the nanoscale range with uniform size distribution. The TEM results revealed smaller particles and higher dispersion of Ni particles in promoted catalyst. The portion of larger particles is higher in unpromoted catalyst.

Catalytic performance

The CO_2 conversion, CO and CH_4 selectivity over Ni/Al_2O_3 at different temperatures are shown in Fig. 7a–c, respectively. The results showed that with increasing the nickel content up to 5%, CO_2 conversion increased. Increasing the nickel content higher than 5% did not have much effect on catalyst activity and it just increased the methanation. Two percent showed lowest catalytic activity and highest CO selectivity in comparison with other Ni loadings. High activity and CO selectivity of 5Ni (in comparison with 7Ni and 10Ni) is due to higher dispersion or incorporation of Ni species with the Al_2O_3 support. Ni species with low dispersity and large particles and an increase in H_2 coverage on active sites, which is in favor of CH_4 formation ($CO_2 + 4H_2 \leftrightarrow CH_4 + 2H_2O$) [15, 17]. To evaluate the effect of promoter on CO selectivity, we chose 5% nickel to proceed.

The CO_2 conversion and CO selectivity of alkali and rare earth promoted 5% Ni/Al_2O_3 catalysts are presented in Fig. 8a–d, respectively. Results showed that addition of rare earth metal or alkali promoters decreased the catalytic activity at 400 °C, but at higher temperatures they exhibited almost the same activity and even higher. The lower activity at temperatures below 500 °C is related to decrease of methanation reactions occurring along with the RWGS reaction. In other words, there is no decrease in RWGS catalytic activity and this decrease is attributed to decrease of side reactions. Among the alkali and rare earth promoted catalysts 1% La and 2% K showed higher CO_2 conversion especially at temperatures higher than 500 °C.

CH_4 formation was reduced during the reaction for all the promoted catalysts. One percent Ce increased CO selectivity by about 4%, 1% Mg and 1% La by about 9% and 1% K by about 20% at 400 °C. After that the results of 1% promoters were obtained, we continued our work with 2% La and 2% K on 5% Ni/Al_2O_3. Two percent K decreased the catalytic activity and methanation more than 1% K, where 2%

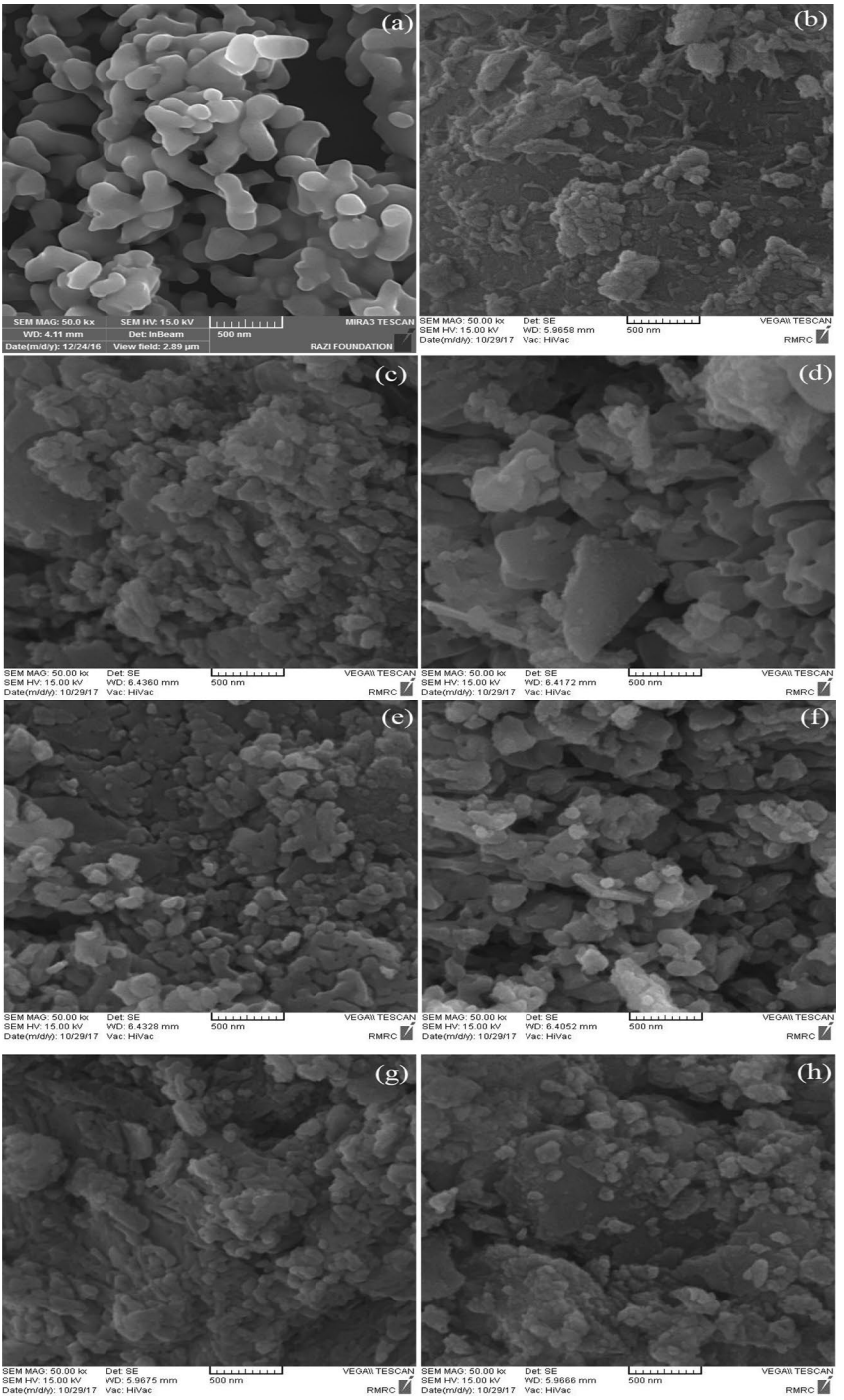

Fig. 5 SEM images of prepared support and catalysts; **a** Al_2O_3, **b** $5Ni/Al_2O_3$, **c** $5Ni–1Ce/Al_2O_3$, **d** $5Ni–1Mg/Al_2O_3$, **e** $5Ni–1La/Al_2O_3$, **f** $5Ni–2La/Al_2O_3$, **g** $5Ni–1K/Al_2O_3$, **h** $5Ni–2K/Al_2O_3$

Table 4 Elemental composition of promoted catalysts detected by EDS analysis

Element	5Ni–1Ce		5Ni–1Mg		5Ni–1La		5Ni–2K	
	(wt%)	(at.%)	(wt%)	(at.%)	(wt%)	(at.%)	(wt%)	(at.%)
O	55.12	68.83	58.28	71.52	57.52	71.07	54.60	68.46
Al	39.87	29.52	34.94	25.42	37.45	27.44	39.68	29.49
Ni	4.59	1.60	5.10	1.70	3.98	1.34	3.93	1.23
Ce	0.43	0.08	–	–	–	–	–	–
Mg	–	–	1.68	1.36	–	–	–	–
La	–	–	–	–	1.05	0.15	–	–
K	–	–	–	–	–	–	1.59	0.81

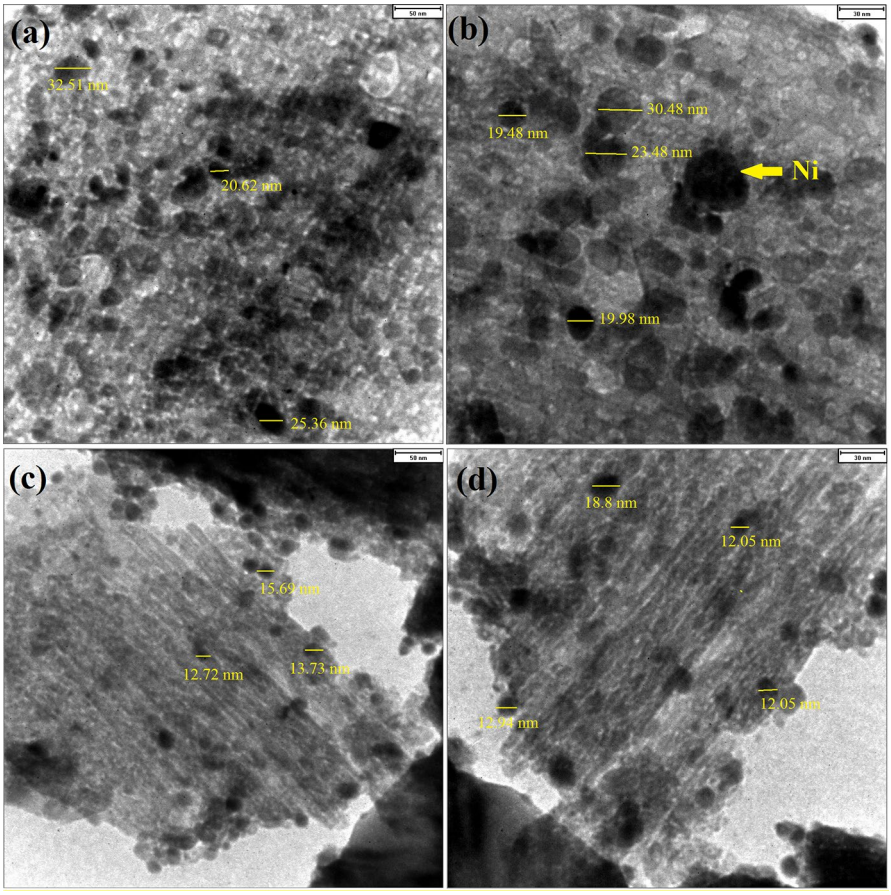

Fig. 6 TEM images of reduced catalysts; **a**, **b** 5Ni/Al_2O_3, **c**, **d** 5Ni–2K/Al_2O_3

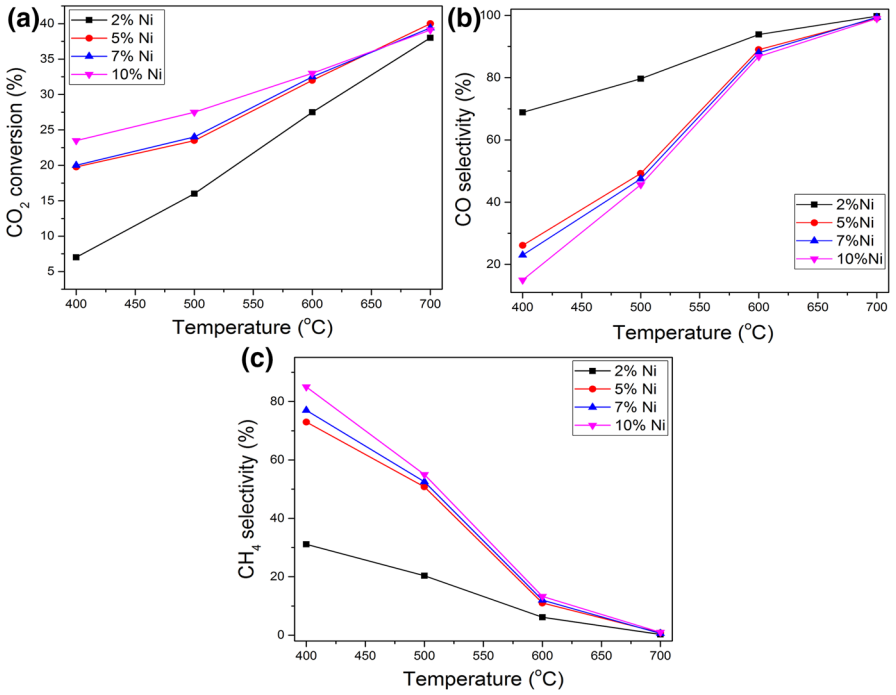

Fig. 7 **a** CO_2 conversion, **b** CO selectivity and **c** CH_4 selectivity of Ni/Al_2O_3 catalysts at different temperatures, H_2:CO_2 = 1:1 (GHSV = 1.5×10^4 ml g^{-1} h^{-1})

La in comparison with 1% La showed almost the same activity and lower CO selectivity. In general, the CO selectivity of catalysts exhibited the following order: 2K > 1K > 1La > 1Mg > 2La > 1Ce.

The obtained results are great in agreement with the literature. Better catalytic activity of promoted catalysts due to surface rearrangement is stated by many researchers [39–41]. The catalytic activity of un-modified $5Ni/Al_2O_3$ has been previously reported; the reported catalyst showed CO_2 conversion of 32% and CO selectivity less than 78% at 600 °C [42]. In this study we have CO_2 conversion of about 35% and CO selectivity higher than 90% for the promoted catalysts at 600 °C. Literature reports emphasize the exceptional role of the supports with oxygen storage ability and their effect on catalytic activity [16, 21]. These catalysts showed high CO selectivity at low Ni loadings, but by increasing the Ni content the CO selectivity decreased. The same results were reported for the Ni catalysts supported on SiO_2 and Al_2O_3 [15, 17, 20]. Here we can conclude that for Ni based catalysts the size of Ni particles and their dispersity plays a much more important role in CO selectivity. Nickel species with high dispersion and small particle size are in favor of RWGS reaction, where large and agglomerated nickel particles put forward the CO_2 methanation reaction [15]. Comparing the promoted Ni/Al_2O_3 catalysts with the reported catalysts, these cost effective catalysts seem to be very promising catalyst for RWGS reaction. Promoted Ni/Al_2O_3 catalysts exhibit high activity and CO selectivity for

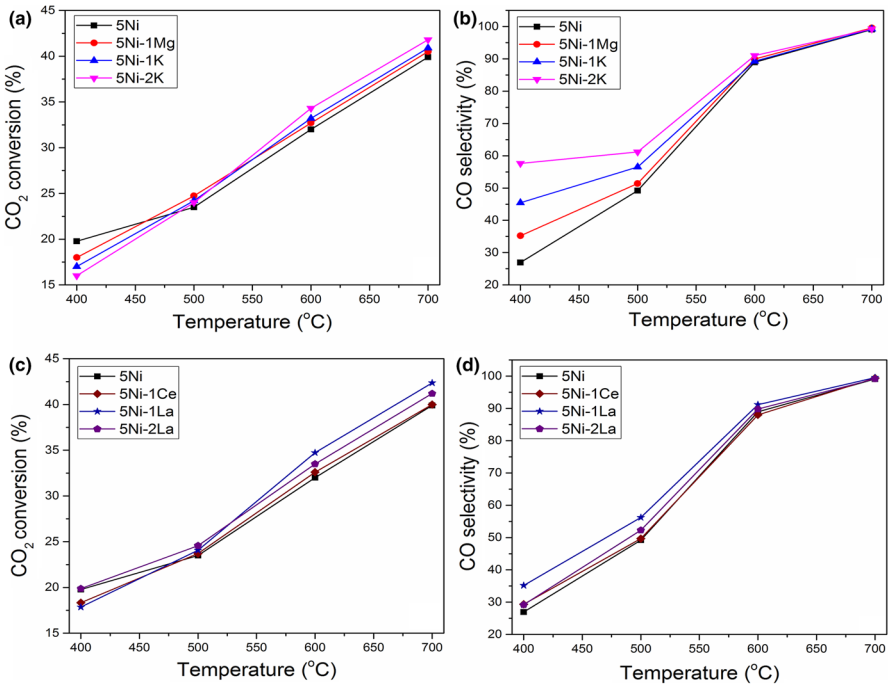

Fig. 8 **a**, **b** CO_2 conversion and CO selectivity of alkali promoted catalysts (5Ni-M/Al_2O_3 (M = Mg, K)), **c**, **d** CO_2 conversion and CO selectivity of rare earth promoted catalysts (5Ni-M/Al_2O_3 (M = Ce, La)) at different temperatures, H_2:CO_2 = 1:1 (GHSV = 1.5×10^4 ml g^{-1} h^{-1})

the titled reaction; this can be accredited to the increase of Ni dispersion, concentration of surface active sites and CO_2 adsorption by basic nature of promoters.

The obtained results in this research encourage the importance of Ni dispersity and size in catalytic activity and CO selectivity in RWGS reaction. Addition of promoters especially using co-impregnation technique improves Ni dispersity and reducibility, as stated by Koo et al. [43]. The increase of Ni dispersity and reducibility of promoted catalysts were confirmed with TPR results (Fig. 4). The TPR profiles of promoted catalysts showed an additional peak at 380 °C related to well disperse NiO species. The TPR results indicated increase of H_2 consumption in promoted catalysts. Smaller Ni particle size and higher dispersion of 5Ni promoted catalysts were also confirmed by TEM images (Fig. 6). TEM images of 5Ni–2K showed smaller Ni particles and higher dispersion in comparison with unpromoted 5Ni catalyst.

On the other hand, addition of a basic promoter enhances the CO_2 adsorption and formation of formates. Formate dissociation mechanism is the leading

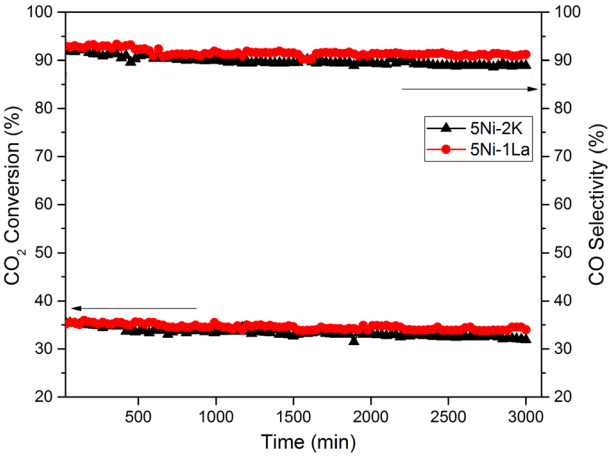

Fig. 9 The long-term stability over 5Ni–2K and 5Ni–1La, reaction temperature: 600 °C, H_2:CO_2 = 1:1 (GHSV = 1.5×10^4 ml g^{-1} h^{-1})

mechanism proposed for production of CO from RWGS reaction [44, 45]. The possible mechanism over promoted catalysts is as follows; firstly, CO_2 gas is adsorbed on Ni, interfaces of Ni–K, while H_2 is adsorbed and dissociated only by nickel to H. Secondly, the hydrogen atoms on Ni associate with CO_2 available on the Ni surface or the CO_2 adsorbed by on the interfaces of Ni–K to form formates. Finally, by decomposition of formates CO is formed and hydrogen atoms associate with OH to form H_2O.

Chen et al. reported the increase of CO_2 adsorption after impregnation of the catalyst with K by using CO_2-TPD analysis [12]. Addition of K to Cu/Al_2O_3 catalyst increased the CO_2 adsorption and CO selectivity up to 95.8% at pressures higher than 10 Mpa [46]. Increase of the basicity of alumina support after addition of an alkali or rare earth promoter (Mg and La) was also confirmed by Koo et al. [36]. High H_2 adsorption puts forward the CO_2 methanation reaction, while a decrease in hydrogen coverage and increase in CO_2 adsorption is in favor of RWGS reaction.

The long-term stability tests were performed on 1% La and 2% K, see Fig. 9. Both catalysts performed great catalytic activity and CO selectivity during 50 h on stream. One percent La showed about 1% decrease in CO_2 conversion and CO selectivity after 50 h, while 2% K exhibited about 3% decrease.

The SEM images of 5Ni–2K and 5Ni–1La after 15 h on stream and TEM image of 5Ni–2K after 50 h on stream are shown in Fig. 10. The SEM images confirmed stable catalytic structure after 15 h on stream (Fig. 10a, b). No sintering of particles is noticed for both catalysts. The TEM image of spent 5Ni–2K showed no particular changes (Fig. 10c) and stable catalyst structure is detected after 50 h on stream. The spent catalyst showed only a small increase in Ni size after the stability test.

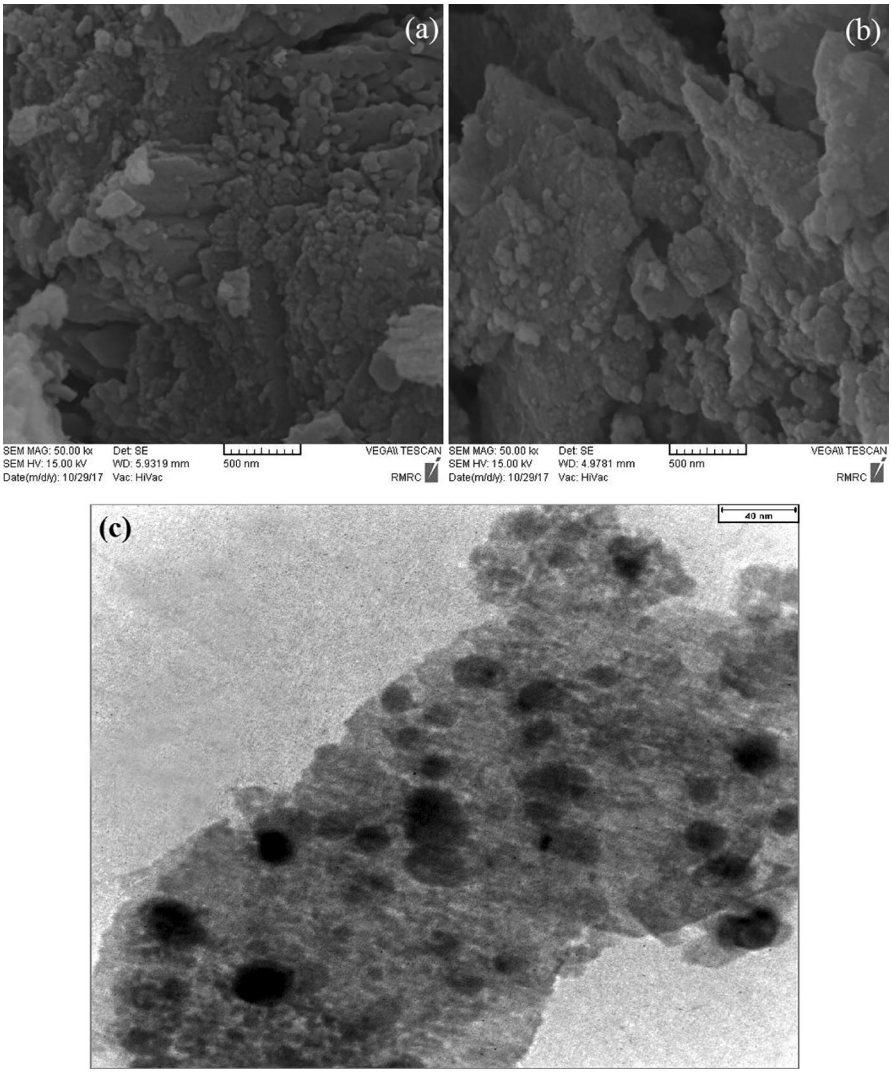

Fig. 10 images of spent catalysts; **a**, **b** SEM images of 5Ni–1La/Al_2O_3, 5Ni–2K/Al_2O_3 after 15 h on stream and **c** TEM image of 5Ni–2K after 50 h on stream, reaction temperature: 600 °C, $H_2/CO_2 = 1$, GHSV = 1.5×10^4 ml g^{-1} h^{-1}

Conclusions

Five percent Ni/Al_2O_3 catalyst was impregnated with Ce, La, Mg or K and introduced to increase the CO selectivity and catalytic activity of this catalyst. The promoted Ni catalysts prepared by co-impregnation method showed mesoporous structure and great catalytic activity in reverse water gas shift reaction (RWGS). Addition of rare earth metal (Ce, La) or alkali promoter (Mg, K) to 5Ni/Al_2O_3 reduced the

CO_2 conversion at lower temperatures but increased the CO selectivity up to 30% for 2% K at 400 °C. At higher temperatures, CO_2 conversion increased with addition of promoters. Addition of an alkali or rare earth metal promoter by co-impregnation technique enhanced the dispersity of Ni species on the support, besides increasing the CO_2 adsorption on the surface of catalyst. Addition of 1% La, 1% K and 2% K increased the CO_2 conversion of $5Ni/Al_2O_3$ from 39.8% to 43.2%, 42.5% and 41.8% at 700 °C, respectively. The long-term stability test over 5Ni–1La and 5Ni–2K showed less than 3% decrease in catalytic activity after 50 h on stream.

References

1. B. Liang, H. Duan, X. Su, X. Chen, Y. Huang, X. Chen, T. Zhang, Catal. Today **281**, 319 (2017)
2. S.S. Kim, H.H. Lee, S.C. Hong, Appl. Catal. A Gen. **423**, 100 (2012)
3. M.D. Porosoff, J.G. Chen, J. Catal. **301**, 30 (2013)
4. S.S. Kim, H.H. Lee, S.C. Hong, Appl. Catal. B Environ. **119**, 100 (2012)
5. D.J. Pettigrew, D.L. Trimm, N.W. Cant, Catal. Lett. **28**, 313 (1994)
6. I. Ro, R. Carrasquillo-Flores, J.A. Dumesic, G.W. Huber, Appl. Catal. A Gen. **521**, 182 (2016)
7. W. Wang, S. Wang, X. Ma, J. Gong, Chem. Soc. Rev. **40**, 3703 (2011)
8. A.G. Kharaji, A. Shariati, M.A. Takassi, Chin. J. Chem. Eng. **21**, 1007 (2013)
9. L. Wang, H. Liu, Y. Chen, S. Yang, Int. J. Hydrogen Energy **42**, 3682 (2017)
10. F.S. Stone, D. Waller, Top. Catal. **22**, 305 (2003)
11. C.S. Chen, W.H. Cheng, S.S. Lin, Appl. Catal. A Gen. **257**, 97 (2004)
12. C.S. Chen, W.H. Cheng, S.S. Lin, Appl. Catal. A Gen. **238**, 55 (2003)
13. M. Lortie, Reverse water gas shift reaction over supported Cu–Ni nanoparticle catalysts. Doctoral dissertation, Université d'Ottawa/University of Ottawa, Ottawa, Canada (2014)
14. Y. Liu, Z. Li, H. Xu, Y. Han, Catal. Commun. **76**, 1 (2016)
15. H.C. Wu, Y.C. Chang, J.H. Wu, J.H. Lin, I.K. Lin, C.S. Chen, Catal. Sci. Technol. **5**, 4154 (2015)
16. W.A. Luhui, S. Zhang, L.I. Yuan, J. Rare Earth **26**, 66 (2008)
17. B. Lu, K. Kawamoto, J. Environ. Chem. Eng. **1**, 300 (2013)
18. M.D. Porosoff, S. Kattel, W. Li, P. Liu, J.G. Chen, Chem. Commun. **51**, 6988 (2015)
19. W.A. Luhui, L. Hui, L. Yuan, C.H. Ying, Y.A. Shuqing, J. Rare Earth **31**, 559 (2013)
20. C.S. Chen, J.H. Lin, J.H. You, K.H. Yang, J. Phys. Chem. A **114**, 3773 (2009)
21. F.M. Sun, C.F. Yan, C.Q. Guo, S.L. Huang, Int. J. Hydrogen Energy **40**, 15985 (2015)
22. A. Irankhah, F. Heidari, Y. Davoodbeygi, Res. Chem. Intermed. **43**, 7119 (2017)
23. M.L. Ang, U. Oemar, Y. Kathiraser, E.T. Saw, C.H.K. Lew, Y. Du, S. Kawi, J. Catal. **329**, 130 (2015)
24. C.S. Chen, J.H. You, C.C. Lin, J. Phys. Chem. C **115**, 1464 (2011)
25. Z. Alipour, M. Rezaei, F. Meshkani, J. Ind. Eng. Chem. **20**, 2858 (2014)
26. N.D. Charisiou, G. Siakavelas, K.N. Papageridis, A. Baklavaridis, L. Tzounis, D.G. Avraam, M.A. Goula, J. Nat. Gas Sci. Eng. **31**, 164 (2016)
27. F. Meshkani, S.F. Golesorkh, M. Rezaei, M. Andache, Res. Chem. Intermed. **43**, 545 (2017)
28. M.A. Goula, N.D. Charisiou, G. Siakavelas, L. Tzounis, I. Tsiaoussis, P. Panagiotopoulou, G. Goula, I.V. Yentekakis, Int. J. Hydrogen Energy **42**, 13724 (2017)
29. Y.H. Park, J.Y. Kim, D.J. Moon, N.C. Park, Y.C. Kim, Res. Chem. Intermed. **41**, 9603 (2015)
30. J. Mazumder, H.I. de Lasa, Catal. Today **237**, 100 (2014)
31. M. Bettman, R.E. Chase, K. Otto, W.H. Weber, J. Catal. **117**, 447 (1989)
32. M. Thommes, K. Kaneko, A.V. Neimark, J.P. Olivier, F. Rodriguez-Reinoso, J. Rouquerol, K.S. Sing, Pure Appl. Chem. **87**, 1051 (2015)
33. L. Zhang, X. Wang, C. Chen, X. Zou, X. Shang, W. Ding, X. Lu, RSC Adv. **7**, 33143 (2017)
34. J. Li, Y. Ren, B. Yue, H. He, Chin. J. Catal. **38**, 1166 (2017)
35. T. Osaki, T. Mori, J. Catal. **204**, 89 (2001)
36. K.Y. Koo, H.S. Roh, Y.T. Seo, D.J. Seo, W.L. Yoon, S.B. Park, Appl. Catal. A Gen. **340**, 183 (2008)

37. Y.X. Zeng, L. Wang, C.F. Wu, J.Q. Wang, B.X. Shen, X. Tu, Appl. Catal. B Environ. **224**, 469 (2018)
38. A. Goguet, F.C. Meunier, D. Tibiletti, J.P. Breen, R. Burch, J. Phys. Chem. B **108**, 20240 (2004)
39. M. García-Diéguez, C. Herrera, M.Á. Larrubia, L.J. Alemany, Catal. Today **197**, 50 (2012)
40. M.H. Amin, S. Putla, S.B.A. Hamid, S.K. Bhargava, Appl. Catal. A Gen. **492**, 160 (2015)
41. Y. Jiao, Y. Du, J. Zhang, C. Li, Y. Xue, J. Lu, Y. Chen, J. Anal. Appl. Pyrolysis **116**, 58 (2015)
42. S. Choi, B.I. Sang, J. Hong, K.J. Yoon, J.W. Son, J.H. Lee, B.K. Kim, Sci. Rep. **7**, 41207 (2017)
43. K.Y. Koo, H.S. Roh, U.H. Jung, W.L. Yoon, Catal. Today **185**, 126 (2012)
44. A. Goguet, F. Meunier, J. Breen, R. Burch, M.I. Petch, A.F. Ghenciu, J. Catal. **226**, 382 (2004)
45. R. Yang, C. Xing, C. Lv, L. Shi, N. Tsubaki, Appl. Catal. A Gen. **385**, 92 (2010)
46. B. Atul, B. Tidona, Ph. Rudolf von Rohr, A. Urakawa, Catal. Sci. Technol. **3**, 767 (2013)